

Magnetotransport properties of large-scale $PtTe_2$ Dirac semimetal films grown by pulsed laser deposition

Zhongqiang Chen(陈中强), Zhe Wang(王喆), Kankan Xu(徐侃侃), Xu Zhang(张旭), Ruijie Xu(徐睿劼), and Xuefeng Wang(王学锋)

Citation: Chin. Phys. B, 2025, 34 (**7**): 077401. DOI: 10.1088/1674-1056/adcf8c
http://cpb.iphy.ac.cn; http://iopscience.iop.org/cpb

What follows is a list of articles you may be interested in

Optimization of large-area $YBa_2Cu_3O_{7-\delta}$ thin films by pulsed laser deposition for planar microwave devices

Pei-Yu Xiong(熊沛雨), Fu-Cong Chen(陈赋聪), Zhong-Pei Feng(冯中沛), Jing-Ting Yang(杨景婷), Yu-Dong Xia(夏钰东), Yue-Feng Yuan(袁跃峰), Xu Wang(王旭), Jie Yuan(袁洁), Yun Wu(吴云), Jing Shi(石兢), and Kui Jin(金魁)
Chin. Phys. B, 2023, 32 (**7**): 077402. DOI: 10.1088/1674-1056/accb4d

Enhancing superconductivity of ultrathin $YBa_2Cu_3O_{7-\delta}$ films by capping non-superconducting oxides

Hai Bo(薄海), Tianshuang Ren(任天爽), Zheng Chen(陈峥), Meng Zhang(张蒙), Yanwu Xie(谢燕武)
Chin. Phys. B, 2019, 28 (**6**): 067402. DOI: 10.1088/1674-1056/28/6/067402

Electronic structure and nematic phase transition in superconducting multiple-layer FeSe films grown by pulsed laser deposition method

Bing Shen(沈兵), Zhong-Pei Feng(冯中沛), Jian-Wei Huang(黄建伟), Yong Hu(胡勇), Qiang Gao(高强), Cong Li(李聪), Yu Xu(徐煜), Guo-Dong Liu(刘国东), Li Yu(俞理), Lin Zhao(赵林), Kui Jin(金魁), X J Zhou(周兴江)
Chin. Phys. B, 2017, 26 (**7**): 077402. DOI: 10.1088/1674-1056/26/7/077402

Observation of selective surface element substitution in $FeTe_{0.5}Se_{0.5}$ superconductor thin film exposed to ambient air bysynchrotron radiation spectroscopy

Nian Zhang(张念), Chen Liu(刘晨), Jia-Li Zhao(赵佳丽), Tao Lei(雷涛), Jia-Ou Wang(王嘉鸥), Hai-Jie Qian(钱海杰), Rui Wu(吴蕊), Lei Yan(颜雷), Hai-Zhong Guo(郭海中), Kurash Ibrahim(奎热西)
Chin. Phys. B, 2016, 25 (**9**): 097402. DOI: 10.1088/1674-1056/25/9/097402

Fabrication and properties of high performance $YBa_2Cu_3O_{7-\delta}$ radio frequency SQUIDs with step-edge Josephson junctions

Liu Zheng-Hao (刘政豪), Wei Yu-Ke (魏玉科), Wang Da (王达), Zhang Chen (张琛), Ma Ping (马平), Wang Yue (王越)
Chin. Phys. B, 2014, 23 (**9**): 097401. DOI: 10.1088/1674-1056/23/9/097401

RAPID COMMUNICATION

Magnetotransport properties of large-scale $PtTe_2$ Dirac semimetal films grown by pulsed laser deposition

Zhongqiang Chen(陈中强), Zhe Wang(王喆), Kankan Xu(徐侃侃), Xu Zhang(张旭), Ruijie Xu(徐睿劼), and Xuefeng Wang(王学锋)†

National Key Laboratory of Spintronics, Jiangsu Provincial Key Laboratory of Advanced Photonic and Electronic Materials, School of Electronic Science and Engineering, and Collaborative Innovation Center of Advanced Microstructures, Nanjing University, Nanjing 210093, *China*

(Received 11 April 2025; revised manuscript received 17 April 2025; accepted manuscript online 23 April 2025)

Type-II Dirac semimetal $PtTe_2$ is a promising candidate for various electronic device applications due to its high carrier mobility, high conductivity, and air stability. In this work, we report on the growth of large-scale $PtTe_2$ films by the pulsed laser deposition (PLD) and the comparison of the magnetotransport properties with the $PtTe_2$ films grown by the chemical vapor deposition (CVD). The low-temperature Hall curves of the PLD-grown films exhibit a linear behavior, in contrast with the nonlinear characteristic of the Hall behavior observed in CVD-grown films, in which a defect gradient is introduced. Meanwhile, both $PtTe_2$ films show weak antilocalization at low temperatures, which is attributed to the strong spin–orbit coupling.

Keywords: $PtTe_2$, pulsed laser deposition, magnetotransport properties, thin films

PACS: 74.78.Fk, 75.30.Gw, 75.47.Lx, 75.70.–i

DOI: 10.1088/1674-1056/adcf8c **CSTR:** 32038.14.CPB.adcf8c

1. Introduction

Transition-metal dichalcogenides (TMDs) provide excellent platforms for exploration of the next-generation electronics,[1–4] optoelectronics,[5–8] and spintronics[9–12] due to their unique structures and distinctive properties. Since the exfoliation with limited controllability is incompatible with practical industrial applications,[13–16] large-scale epitaxial films can be used to construct heterostructures more flexibly.[17–21] Recently, TMD films grown by the pulsed laser deposition (PLD) have developed rapidly with the advantages of high growth rate, low growth temperature and controllable thickness.[22–25] For example, the large-area WTe_2 films showed distinct Shubnikov–de Haas oscillations and tunable magnetoresistance,[26,27] even after being transferred to other substrates.[28] In the large-scale Cr_xTe_y films, the concentration of Cr intercalation changed the topological spin textures and the Curie temperature.[29–31] Besides, when the PLD-grown topological materials were constructed to form ferromagnetic heterostructures, they demonstrated remarkable spin-to-charge conversion.[32,33] Therefore, it is highly desirable to extend the PLD technique to the growth of other TMD films for the fundamental studies and scalable applications.

$PtTe_2$, as an emergent type-II Dirac semimetal,[34–36] exhibits a giant spin Hall conductivity due to its large spin–orbit torque efficiency and high conductivity.[37,38] The $PtTe_2$ films with controllable thickness down to a few layers can be synthesized mainly through chemical vapor deposition (CVD),[39–41] and molecular beam epitaxy (MBE).[35,42] When it combines with WTe_2 to form a van der Waals heterostructure, field-free switching of the perpendicular magnetization can be achieved.[43] Our recent work has demonstrated that the introduction of a defect gradient in $PtTe_2$ films breaks its intrinsic symmetry, thereby inducing the high-efficiency helicity-dependent terahertz emission.[39] Besides, the nearly fully occupied d orbitals of Pt and the highly hybridized p_z orbitals of interlayer Te atoms suggest the strong interlayer interactions and layer-dependent properties in $PtTe_2$ films,[8,35,44] which warrants further investigations of their prominent properties.

In this work, we employ the PLD to grow large-area $PtTe_2$ films, and compare the magnetotransport properties with the CVD-grown $PtTe_2$ films. The conductivity of the $PtTe_2$ films reaches 10^6 S·m^{-1} at room temperature. However, the low-temperature Hall curves of PLD-grown $PtTe_2$ films exhibit a linear characteristic due to the absence of the defect gradient, unlike the CVD-grown films. We further fit the Hall resistance and weak antilocalization (WAL) for quantitative analysis.

2. Methods

For the PLD growth, the target was made by pre-reacted $PtTe_2$ powders. The growth process has been described elsewhere.[45] The x-ray diffraction (XRD) pattern for the $PtTe_2$ target is shown in Fig. S1. The two-step CVD process has also been introduced in our recent work.[39] The thickness

†Corresponding author. E-mail: xfwang@nju.edu.cn

© 2025 Chinese Physical Society and IOP Publishing Ltd. All rights, including for text and data mining, AI training, and similar technologies, are reserved.

was measured by atomic force microscopy (AFM) (SOLVER-P47, NT-MDT), and their crystalline structure was determined by XRD using a Cu K_α line (Bruker D8 Discover) and a micro-Raman spectrometer (NT-MDT nanofinder-30) with a 514.5-nm laser. The composition was determined by x-ray photoelectron spectroscopy (XPS) using a ULVAC-PHI 5000 Versa Probe using Al K_α source. For the fabrication of the Hall bar device, we chose the metal mask with a Hall bar pattern and attached it to the sample surface with the silver glue. Subsequently, the $PtTe_2$ film was etched by a home-made ion beam etching system. The magnetotransport properties of the $PtTe_2$ thin films were measured using a Cryogenic cryogen-free measurement system (CFMS-12) with the applied perpendicular magnetic field up to 12 T.

3. Results and discussion

Figure 1(a) shows the schematic illustration of the PLD growth of large-scale $PtTe_2$ films, which is a highly energetic and thermally non-equilibrium process with the transfer of target elements onto the sapphire substrate.[23,46] An excimer laser is employed to ablate the target material, generating a plasma that expands toward the substrate. This plasma consists of energetic species, which subsequently deposit onto the substrate and contribute to the formation of the $PtTe_2$ films. This process is distinct from the CVD process, as shown in Fig. S2. For the two-step CVD process, the Pt film was pre-deposited on the sapphire substrate and then tellurized. However, during the tellurization process, a diffusion barrier is formed along the van der Waals gap that restricts the diffusion of Te atoms to some extent, which leads to the formation of a Te-vacancy defect gradient along the depth orientation.[39] Although a defect gradient is introduced in the CVD-grown $PtTe_2$ films, it is exactly this growth mode that breaks its intrinsic symmetry, thus inducing a nonlinear transport. Besides, to improve the understanding of thin film growth process by the PLD, the reflection high-energy electron diffraction (RHEED) can serve as a valuable tool for the real-time monitoring of the growth dynamics throughout the deposition. The RHEED pattern as a function of time for the $PtTe_2$ films is shown in Fig. 1(b), which is difficult to achieve in a CVD system. Before the film deposition, the RHEED pattern shows the bright spots of the sapphire substrate. During the film deposition, the substrate spots disappear as the bright streaks emerge, indicating the formation of the high-quality $PtTe_2$ films. Therefore, we can obtain $PtTe_2$ films with desirable properties by choosing the appropriate preparation methods.

The Raman spectra of $PtTe_2$ films with different thickness are shown in Fig. 2(a), and the thickness is measured by AFM (Fig. S3). All the samples have two peaks at 111 cm^{-1} and 157 cm^{-1}, corresponding to different vibration modes of the $PtTe_2$ lattice. The peak at around 111 cm^{-1} is the E_g mode from the in-plane Te–Pt–Te lattice vibration, and the 157 cm^{-1} peak corresponds to the A_{1g} mode from the out-of-plane vibration.[15] The $PtTe_2$ layers are coupled by the van der Waals force, and the interlayer van der Waals force suppresses atomic vibration with the increasing layer number.[47] The corresponding XRD patterns of the $PtTe_2$ films exhibit the evident (00l) characteristic diffraction peaks, indicating a highly ordered crystalline structure [Fig. 2(b)]. The energy dispersive spectrometer (EDS) analysis is also conducted to analyze the proportion of Pt and Te [Figs. 2(c) and 2(d)]. The estimated atomic ratio of Pt to Te is 1:1.96 in an area of 30 μm×15 μm, largely consistent with the results of XPS (Fig. S4). These results indicate that $PtTe_2$ films grown by the PLD are free of the defect gradient.

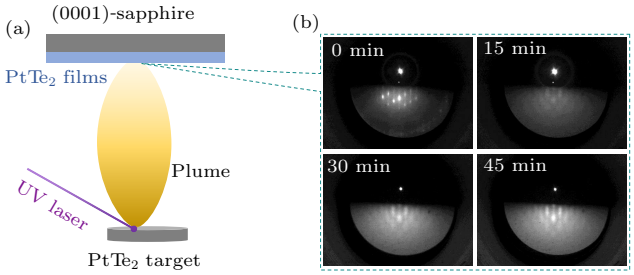


Fig. 1. (a) The schematic illustration for the growth of the large-scale $PtTe_2$ films by PLD. (b) The RHEED patterns during the deposition.

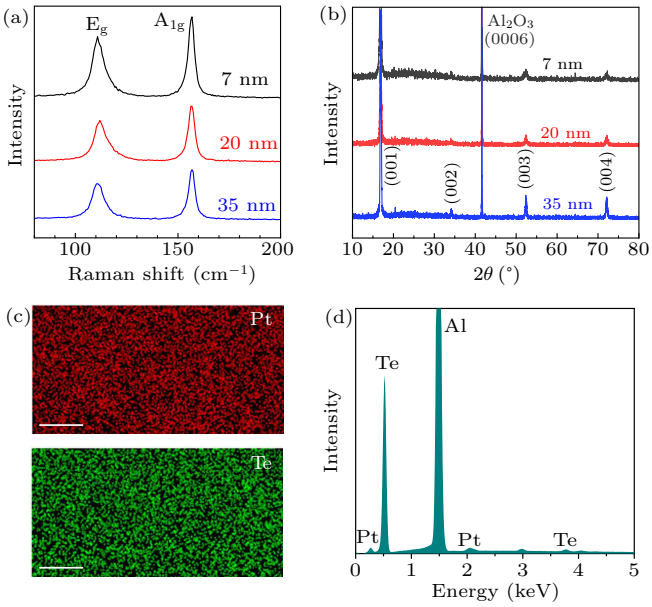


Fig. 2. Structural characterization of $PtTe_2$ films grown by PLD. (a) Raman spectra of $PtTe_2$ films with the thickness of 7 nm, 20 nm and 35 nm. (b) The corresponding XRD patterns for $PtTe_2$ films. (c) The in-plane EDS mapping for the Pt (top panel) and Te element (bottom panel). The scale bar is 5 μm. (d) The corresponding EDS spectrum for the Pt and Te. Pt/Te atomic ratio is estimated to be 1:1.96.

We further investigate the magnetotransport properties of the $PtTe_2$ film at low temperatures. The Hall bar device with a long channel length of ∼ 3 mm is fabricated by ion beam etching. Figure 3(a) shows the temperature-dependent conductivity by the two different methods, which exhibits a metal-

lic property with high electrical conductivity. The residual resistivity ratio (RRR, defined as RRR $= \rho_{300\,\mathrm{K}}/\rho_{5\,\mathrm{K}}$) of the samples grown by the PLD method is 1.90, which is comparable to that of samples grown by the CVD method (~ 1.94). Notably, the PLD-grown samples exhibit a higher conductivity due to the lower defect scattering. When the temperature is reduced to 2 K, the conductivity of the $PtTe_2$ approaches nearly 2.8×10^6 S/m. The Hall curves for the PLD-grown samples show a fully linear characteristic from 5 K to 100 K [Fig. 3(b)]. In contrast, the Hall resistance exhibits a nonlinear characteristic for the CVD-grown samples, suggesting that multiple types of carriers are involved in the conductivity. As the temperature increases, the Hall resistance gradually becomes linear. This difference can be due to the modulation of the energy band near the Fermi level by the Te-vacancy defect gradient. The conductivity in $PtTe_2$ films is mainly contributed by electron carriers. When Te-vacancy defects are introduced, they lead to a downward shift of the Fermi energy level. Then the hole carriers contribute to the conduction, which leads to the nonlinear characteristic of the Hall curves.[39]

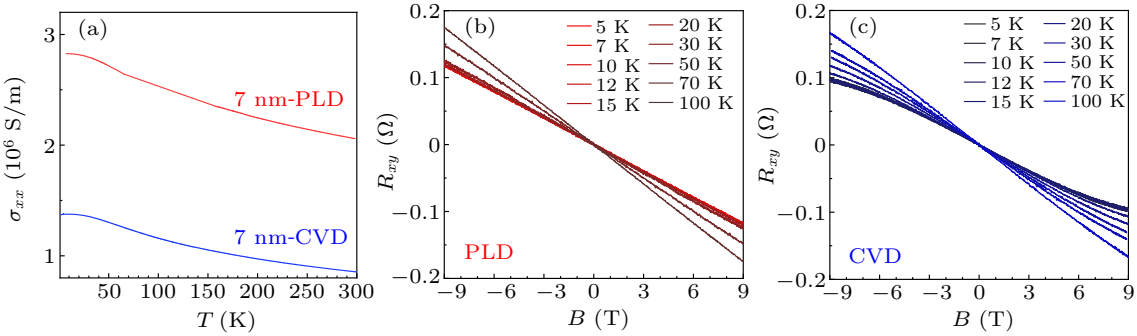


Fig. 3. (a) Temperature-dependent conductivity of the 7-nm-thick $PtTe_2$ films grown by PLD (red curve) and CVD (blue curve), respectively. (b), (c) The Hall curves at various temperatures for the $PtTe_2$ grown by PLD and CVD, respectively.

We perform a quantitative analysis of the Hall measurement for the 7-nm-thick $PtTe_2$ films grown by CVD at 5 K. The Hall resistance is converted to Hall conductivity (σ_{xy}), and a two-band model is applied:

$$\sigma_{xy}(B) = eB\left(\frac{n_\mathrm{h}\mu_\mathrm{h}^2}{1+(\mu_\mathrm{h}B)^2} + \frac{n_\mathrm{e}\mu_\mathrm{e}^2}{1+(\mu_\mathrm{e}B)^2}\right), \tag{1}$$

where e is the electron charge, B is the magnetic field, and n_h, μ_h, n_e and μ_e are the carrier concentrations and the carrier mobilities of hole- and electron-like bands, respectively. We also fit the Hall curves of the PLD samples. The fitting parameters are listed in Table S1.

Figures 4(a) and 4(c) show the magnetoconductance of 7-nm-thick sample grown by PLD and CVD, respectively. The original data of the magnetoresistance are shown in Fig. S5. The magnetic field is applied perpendicular to the film plane. The typical signature of WAL is significant at low temperatures, and this phenomenon is generally regarded as a hallmark of strong spin–orbit coupling.[48] The magnetoconductance curves can be fitted by the Hikami–Larkin–Nagaoka (HLN) model[49]

$$\Delta\sigma(B) = \frac{\alpha e^2}{\pi h}\left[\ln\left(\frac{B_\varphi}{B}\right) - \Psi\left(\frac{1}{2}+\frac{B_\varphi}{B}\right)\right], \tag{2}$$

where α and h are the fitting constant and Planck's constant, respectively. The B_φ is the characteristic field for dephasing interaction, which is related to the phase decoherence length $l_\varphi = \sqrt{h}/(8\pi e B_\varphi)$. The Ψ is the digamma function. The model matches our experimental data very well. The extracted l_φ is 150–160 nm at 5 K, which is larger than the thickness of the $PtTe_2$ films, suggesting that the transport occurs in the quantum diffusion system. Interestingly, the l_φ of the two different synthetic methods are almost comparable. The l_φ displays a $T^{-\gamma}$ dependence with $\gamma = 1.07$ for the PLD-grown sample and 0.90 for the CVD-grown sample, as shown in Figs. 4(b) and 4(d), respectively. The value of γ indicates that electron dephasing in these samples is dominated by electron–phonon interaction ($\gamma = 1$) rather than electron–electron interaction ($\gamma = 0.5$).

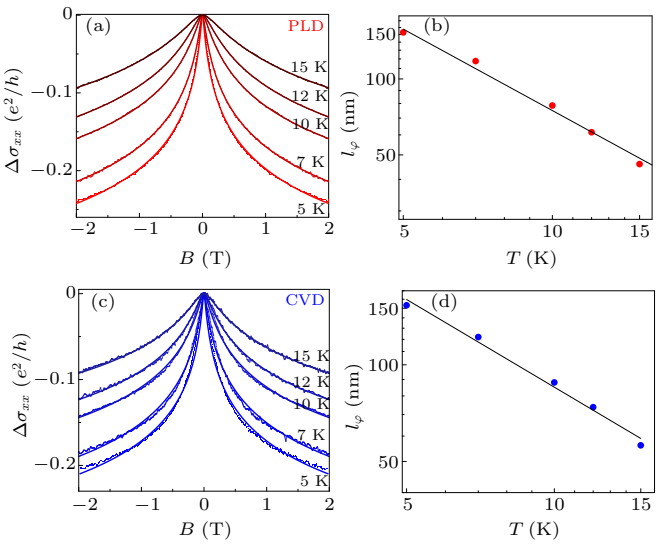


Fig. 4. (a), (c) Magnetoconductance curves at different temperatures of the 7-nm-thick $PtTe_2$ films grown by PLD and CVD, respectively. (b), (d) The corresponding temperature dependence of phase decoherence length. The curves are fitted by $l_\varphi \propto T^{-\gamma}$.

The PLD-grown $PtTe_2$ films show excellent conductivity and strong spin–orbit coupling, which is confirmed by the magnetotransport measurements. The strong spin–orbit coupling makes it highly suitable for spintronics applications. For example, by forming heterostructures like PtTe/$PtTe_2$ through thermal annealing, a giant Rashba spin splitting can be achieved,[50] which is crucial for designing next-generation nanoscale spintronic devices. Additionally, the $PtTe_2$ films can be integrated with superconducting materials to induce a superconducting proximity effect, enabling the development of advanced superconducting electronic devices.

4. Conclusion

In summary, we have grown large-scale $PtTe_2$ films by the PLD and compared the magnetotransport properties with the $PtTe_2$ films grown by the CVD. The results demonstrate that the defect gradient is absent in the PLD-grown $PtTe_2$ films and the WAL effect is dominant at low temperatures. Our work shows that the different growth methods have an impact on the intrinsic properties of the materials, and the PLD is a viable and scalable technique to produce large-scale telluride films for the practical industrial applications.

Acknowledgements

Project supported by the National Key R&D Program of China (Grant No. 2022YFA1402404) and the National Natural Science Foundation of China (Grant Nos. T2394473, 624B2070, and 62274085).

References

[1] Cho S, Kim S, Kim J H, Zhao J, Seok J, Keum D H, Baik J, Choe D H, Chang K J, Suenaga K, Kim S W, Lee Y H and Yang H 2015 *Science* **349** 625

[2] Sung J H, Heo H, Si S, Kim Y H, Noh H R, Song K, Kim J, Lee C S, Seo S Y, Kim D H, Kim H K, Yeom H W, Kim T H, Choi S Y, Kim J S and Jo M H 2017 *Nat. Nanotechnol.* **12** 1064

[3] Zhu W K, Xie S H, Lin H L, Zhang G J, Wu H, Hu T G, Wang Z, Zhang X M, Xu J H, Wang Y J, Zheng Y H, Yan F G, Zhang J, Zhao L X, Patané A, Zhang J, Chang H X and Wang K Y 2022 *Chin. Phys. Lett.* **39** 128501

[4] Chowdhury T, Sadler E C and Kempa T J 2020 *Chem. Rev.* **120** 12563

[5] Ma Q, Krishna Kumar R, Xu S Y, Koppens F H L and Song J C W 2023 *Nat. Rev. Phys.* **5** 170

[6] Ma Q, Grushin A G and Burch K S 2021 *Nat. Mater.* **20** 1601

[7] Sierra J F, Fabian J, Kawakami R K, Roche S and Valenzuela S O 2021 *Nat. Nanotechnol.* **16** 856

[8] Pi L J, Li L, Liu K L, Zhang Q F, Li H Q and Zhai T Y 2019 *Adv. Funct. Mater.* **29** 1904932

[9] Mak K F, Shan J and Ralph D C 2019 *Nat. Rev. Phys.* **1** 646

[10] Jin W, Zhang G J, Wu H, Yang L, Zhang W F and Chang H X 2023 *Chin. Phys. Lett.* **40** 057301

[11] Li H, Ruan S C and Zeng Y J 2019 *Adv. Mater.* **31** e1900065

[12] Duong D L, Yun S J and Lee Y H 2017 *ACS Nano* **11** 11803

[13] Zhou J D, Lin J H, Huang X W, Zhou Y, Chen Y, Xia J, Wang H, Xie Y, Yu H M, Lei J C, Wu D, Liu F C, Fu Q D, Zeng Q S, Hsu C H, Yang C L, Lu L, Yu T, Shen Z X, Lin H, Yakobson B I, Liu Q, Suenaga K, Liu G T and Liu Z 2018 *Nature* **556** 355

[14] Fu L, Hu D B, Mendes R G, Rummeli M H, Dai Q, Wu B, Fu L and Liu Y Q 2018 *ACS Nano* **12** 9405

[15] Ma H F, Chen P, Li B, Li J, Ai R Q, Zhang Z W, Sun G Z, Yao K K, Lin Z Y, Zhao B, Wu R X, Tang X W, Duan X D and Duan X F 2018 *Nano Lett.* **18** 3523

[16] Xu H, Guo C, Zhang J Z, Guo W L, Kuo C N, Lue C S, Hu W D, Wang L, Chen G, Politano A, Chen X S and Lu W 2019 *Small* **15** e1903362

[17] Yadav P, Chen X H, Bhatt S, Das S, Yang H and Mishra R 2024 *Nano Lett.* **24** 2376

[18] Lee W Y, Kang M S, Kim G S, Choi J W, Park N W, Sim Y, Kim Y H, Seong M J, Yoon Y G, Saitoh E and Lee S K 2022 *ACS Nano* **16** 3404

[19] Falson J 2024 *Nat. Mater.* **24** 158

[20] Xue G D, Qin B, Ma C J, Yin P, Liu C and Liu K H 2024 *Chem. Rev.* **124** 9785

[21] Choudhury T H, Zhang X T, Al Balushi Z Y, Chubarov M and Redwing J M 2020 *Annu. Rev. Mater. Res.* **50** 155

[22] Zhuang W Z, Chen Z Q and Wang X F 2022 *Advances in Physics: X* **7** 2034529

[23] Shepelin N A, Tehrani Z P, Ohannessian N, Schneider C W, Pergolesi D and Lippert T 2023 *Chem. Soc. Rev.* **52** 2294

[24] Li X, Liu K X, Wu D, Lin P, Shi Z F, Li X J, Zeng L H, Chai Y, Lau S P and Tsang Y H 2025 *Adv. Mater.* **37** 2415717

[25] Yao J D, Zheng Z Q and Yang G W 2019 *Prog. Mater. Sci.* **106** 100573

[26] Gao M, Zhang M H, Niu W, Chen Y Q, Gu M, Wang H Y, Song F Q, Wang P, Yan S C, Wang F Q, Wang X R, Wang X F, Xu Y B and Zhang R 2017 *Appl. Phys. Lett.* **111** 031906

[27] Chen Y Q, Chen Y D, Ning J A, Chen L M, Zhuang W Z, He L, Zhang R, Xu Y B and Wang X F 2020 *Chin. Phys. Lett.* **37** 017104

[28] Chen Y Q, Liu R X, Chen Y D, Yuan X, Ning J A, Zhang C C, Chen L M, Wang P, He L, Zhang R, Xu Y B and Wang X F 2021 *Chin. Phys. Lett.* **38** 017101

[29] Yang J F, Zhu C, Deng Y, Tang B J and Liu Z 2023 *iScience* **26** 106567

[30] Chen Y Q, Zhu Y M, Lin R J, Niu W, Liu R X, Zhuang W Z, Zhang X, Liang J H, Sun W X, Chen Z Q, Hu Y S, Song F Q, Zhou J, Wu D, Ge B H, Yang H X, Zhang R and Wang X F 2023 *Adv. Funct. Mater.* **33** 2302984

[31] Song A K, Zhang J A, Chen Y Q, Zhang Z Z, Cheng X J, Xu R J, Zhuang W Z, Sun W X, Zhang Y, Zhang X, Chen Z Q, Song F Q, Zhang Y, Zhai X C, Xu Y B, Zhao W S, Zhang R and Wang X F 2025 *Adv. Funct. Mater.* **35** 2422040

[32] Sun W X, Chen Y Q, Zhuang W Z, Chen Z Q, Song A K, Liu R X and Wang X F 2023 *Nanotechnology* **34** 135001

[33] Sun W X, Chen Y Q, Xu R J, Zhuang W Z, Wang D, Liu L, Song A K, Xing G Z, Xu Y B, Zhang R, Chang C Z and Wang X F 2025 *Adv. Funct. Mater.* **35** 2501880

[34] Yan M Z, Huang H Q, Zhang K N, Wang E Y, Yao W, Deng K, Wan G L, Zhang H Y, Arita M, Yang H T, Sun Z, Yao H, Wu Y, Fan S S, Duan W H and Zhou S Y 2017 *Nat. Commun.* **8** 257

[35] Lin M K, Villaos R A B, Hlevyack J A, Chen P, Liu R Y, Hsu C H, Avila J, Mo S K, Chuang F C and Chiang T C 2020 *Phys. Rev. Lett.* **124** 036402

[36] Fu D Z, Bo X Y, Fei F C, Wu B, Gao M, Wang X F, Naveed M, Shah S A, Bu H J, Wang B G, Cao L, Zou W, Wan X G and Song F Q 2018 *Phys. Rev. B* **97** 245109

[37] Xu H J, Wei J W, Zhou H G, Feng J F, Xu T, Du H F, He C L, Huang Y, Zhang J W, Liu Y Z, Wu H C, Guo C Y, Wang X, Guang Y, Wei H X, Peng Y, Jiang W J, Yu G Q and Han X F 2020 *Adv. Mater.* **32** e2000513

[38] Wang M J, Ko T J, Shawkat M S, Han S S, Okogbue E, Chung H S, Bae T S, Sattar S, Gil J, Noh C, Oh K H, Jung Y, Larsson J A and Jung Y 2020 *ACS Appl. Mater. Interfaces* **12** 10839

[39] Chen Z Q, Qiu H S, Cheng X J, Cui J Z, Jin Z M, Tian D, Zhang X, Xu K K, Liu R X, Niu W, Zhou L Q, Qiu T Y, Chen Y Q, Zhang C H, Xi X X, Song F Q, Yu R, Zhai X C, Jin B B, Zhang R and Wang X F 2024 *Nat. Commun.* **15** 2605

[40] Hao S, Zeng J W, Xu T, Cong X, Wang C Y, Wu C C, Wang Y J, Liu X W, Cao T J, Su G X, Jia L X, Wu Z T, Lin Q, Zhang L L, Yan S N, Guo M F, Wang Z L, Tan P H, Sun L T, Ni Z H, Liang S J, Cui X Y and Miao F 2018 *Adv. Funct. Mater.* **28** 1803746

[41] Zhang K N, Wang M, Zhou X, Wang Y, Shen S C, Deng K, Peng H N, Li J H, Lai X B, Zhang L W, Wu Y, Duan W H, Yu P and Zhou S Y 2020 *Nano Res.* **14** 1663
[42] Deng K, Yan M Z, Yu C P, Li J H, Zhou X, Zhang K N, Zhao Y X, Miyamoto K, Okuda T, Duan W H, Wu Y, Zhong X Y and Zhou S Y 2019 *Sci. Bull.* **64** 1044
[43] Wang F, Shi G Y, Kim K W, Park H J, Jang J G, Tan H R, Lin M, Liu Y K, Kim T, Yang D S, Zhao S S, Lee K, Yang S H, Soumyanarayanan A, Lee K J and Yang H 2024 *Nat. Mater.* **23** 768
[44] Voiry D, Mohite A and Chhowalla M 2015 *Chem. Soc. Rev.* **44** 2702
[45] Li Z Y, Chen Y Q, Song A K, Zhang J Z, Zhang R, Zhang Z Z and Wang X F 2024 *Light Sci. Appl.* **13** 181
[46] Choo S, Varshney S, Liu H, Sharma S, James R D and Jalan B 2024 *Sci. Adv.* **10** eadq8561
[47] Wieting T J and Verble J L 1972 *Phys. Rev. B* **5** 1473
[48] Yuan H T, Bahramy M S, Morimoto K, Wu S F, Nomura K, Yang B J, Shimotani H, Suzuki R, Toh M, Kloc C, Xu X D, Arita R, Nagaosa N and Iwasa Y 2013 *Nat. Phys.* **9** 563
[49] Hikami S, Larkin A I and Nagaoka Y 1980 *Prog. Theor. Phys.* **63** 707
[50] Feng R F, Zhang Y, Li J H, Li Q, Bao C H, Zhang H Y, Chen W Y, Tang X, Yaegashi K, Sugawara K, Sato T, Duan W H, Yu P and Zhou S Y 2025 *Nat. Commun.* **16** 2667